Supplemental Figures and figure legends

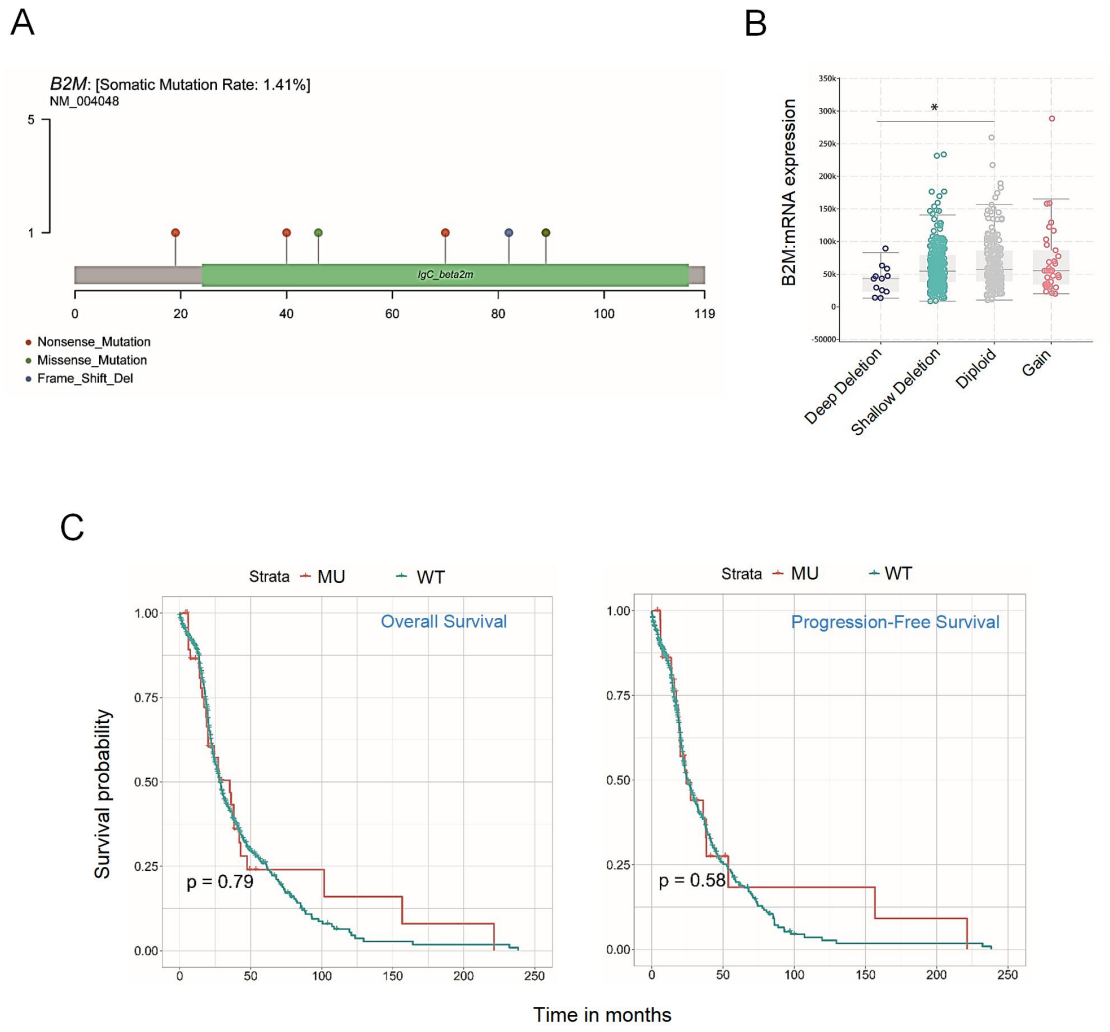

Figure S1. Genetic alterations of the B2M gene in lung cancer. (A) The frequency of *B2M* mutations and the positions and types of *B2M* genetic alterations in the LUAD dataset. (B) The influences of *B2M* CNV on the levels of B2M mRNA in the LUAD dataset. (C) The association between *B2M* mutation status and the survival of LUAD patients.

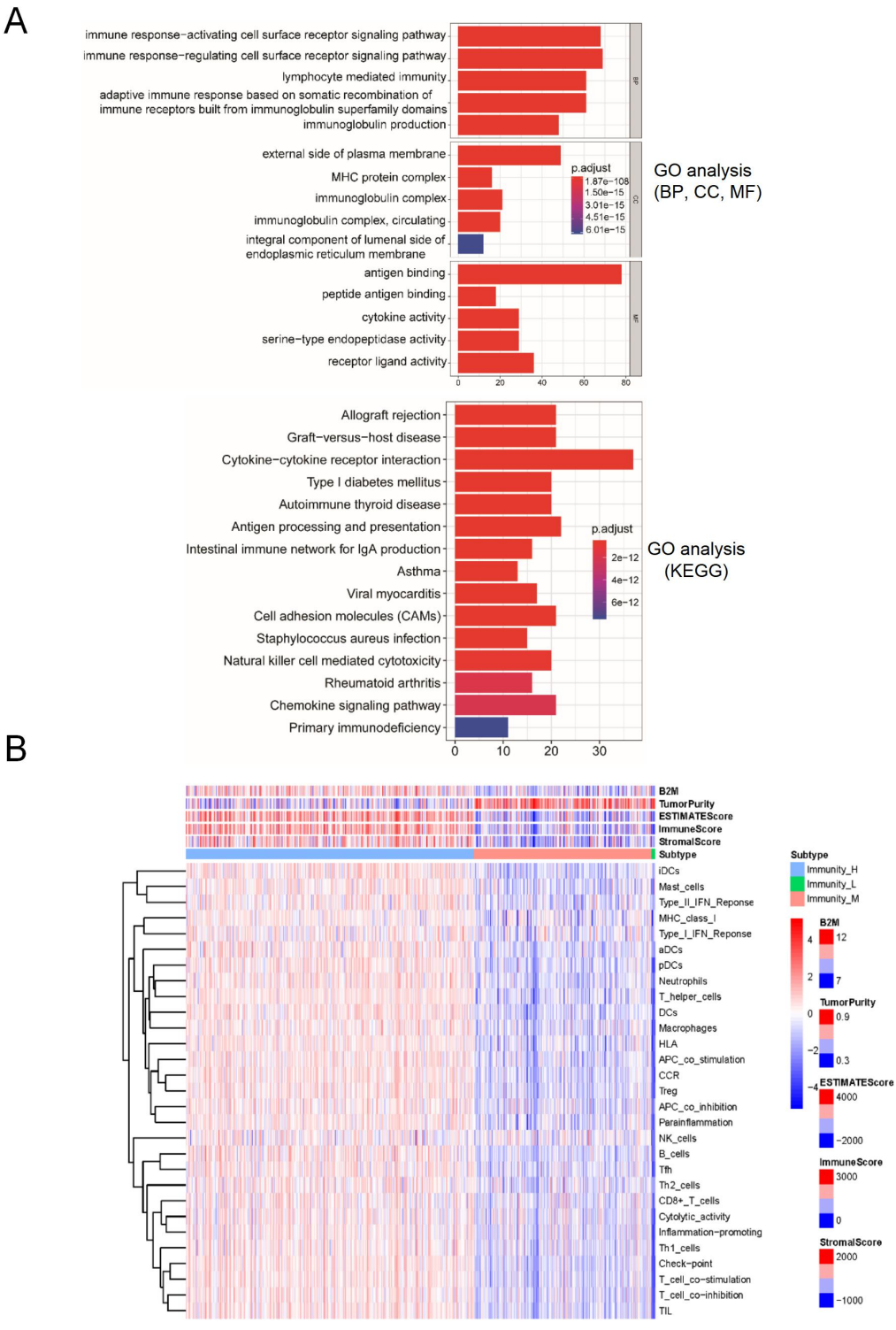

Figure S2. B2M levels impact the immune landscape of lung cancer. (A-B) GO analysis of differentially expressed genes between $B2M^{hi}$ vs. $B2M^{lo}$ tumors in the LUAD dataset. (C) The influence of B2M on the immune-related gene clusters in the LUAD tumors divided into immunity-L, -M, and -H groups.

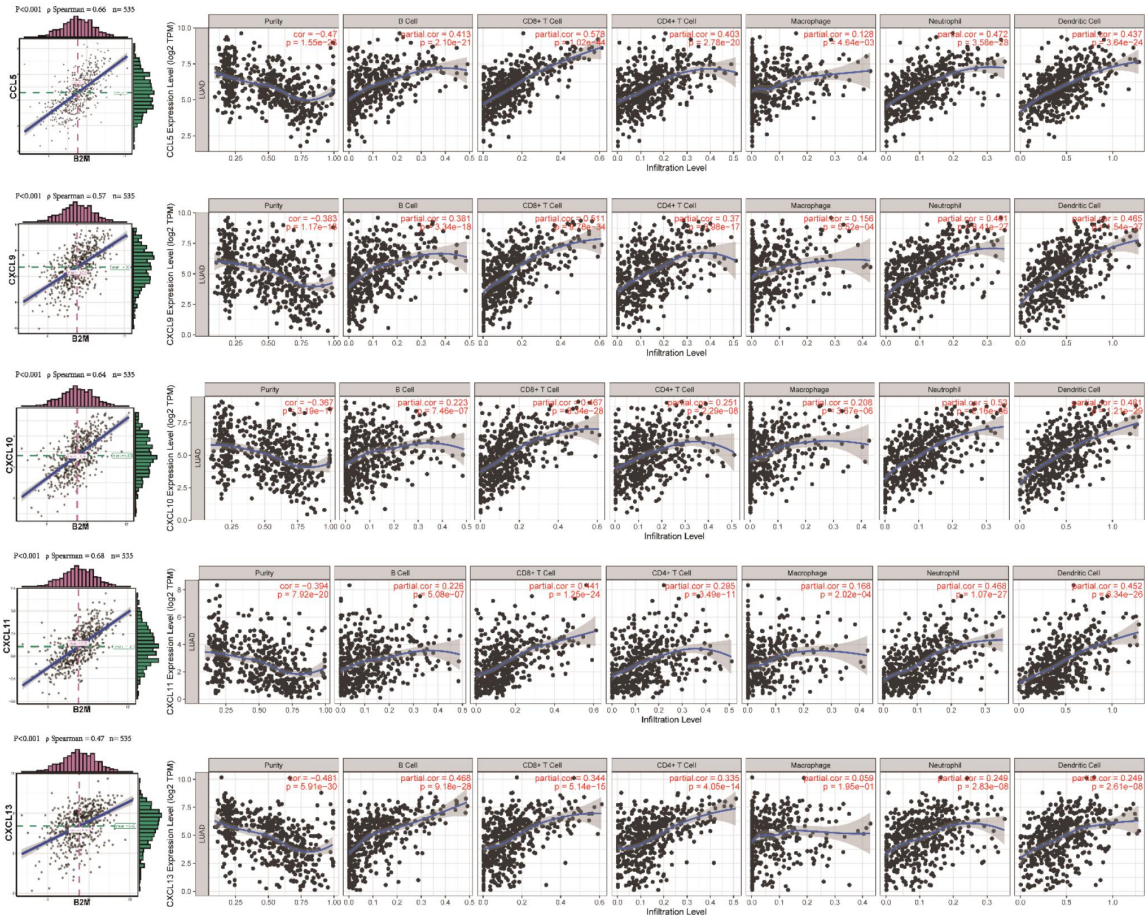

Figure S3. The relationship between B2M and chemokines in lung cancer. Positive correlations between B2M and chemokines, including CCL5, CXCL9, CXCL10, CXCL11, and CXCL13. The correlations between the levels of the indicated chemokines and the infiltration of various immune cell types.

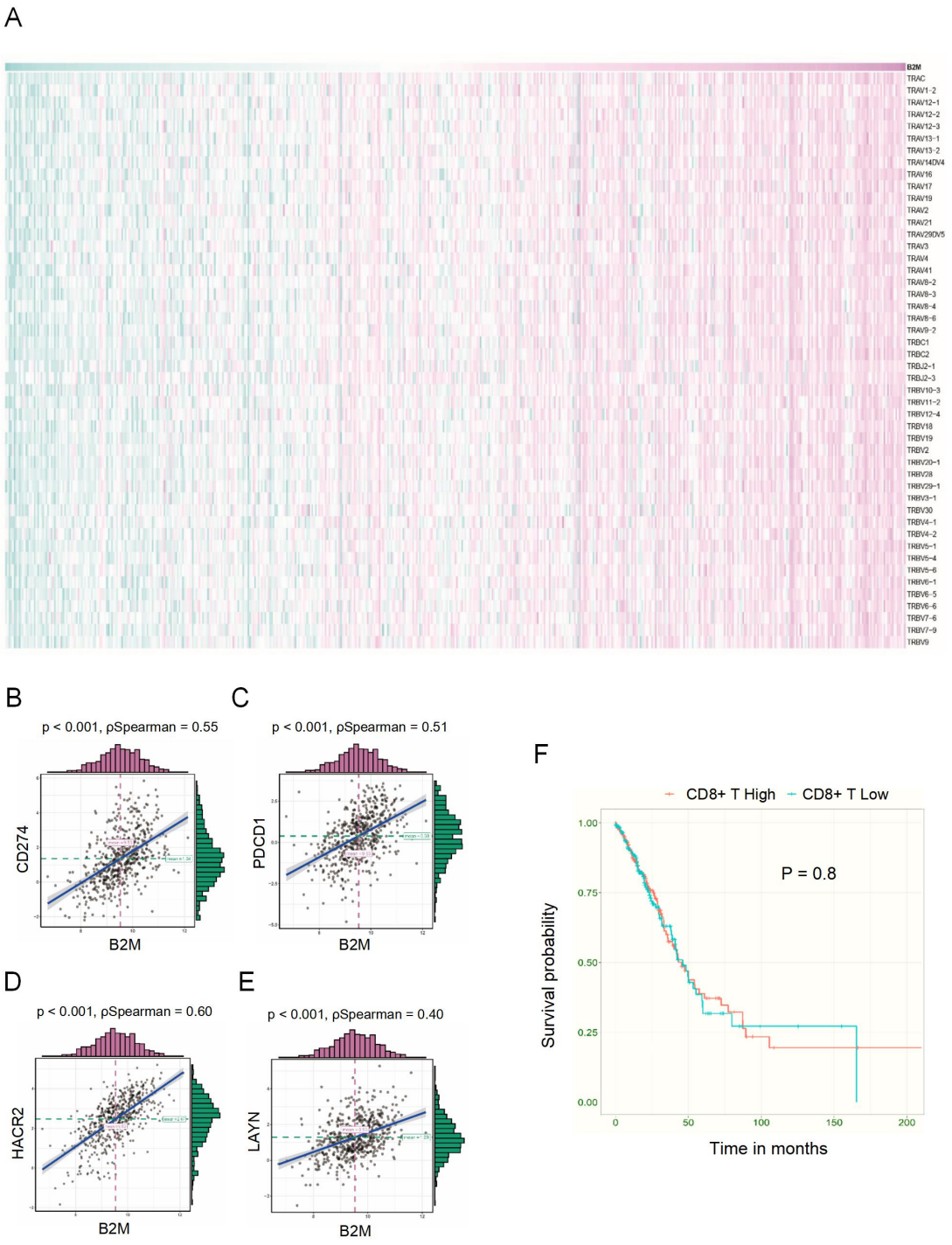

Figure S4. The relationship between B2M levels and T cell recruitment and function. (A) The correlations between the levels of B2M and TCR genes. (B-E) Positive correlations between B2M and T cell immune checkpoint molecules, including CD274, PDCD1, HACR2, and LAYN. (F) The association between the levels of CD8A and the survival time of lung cancer patients in the LUAD dataset.

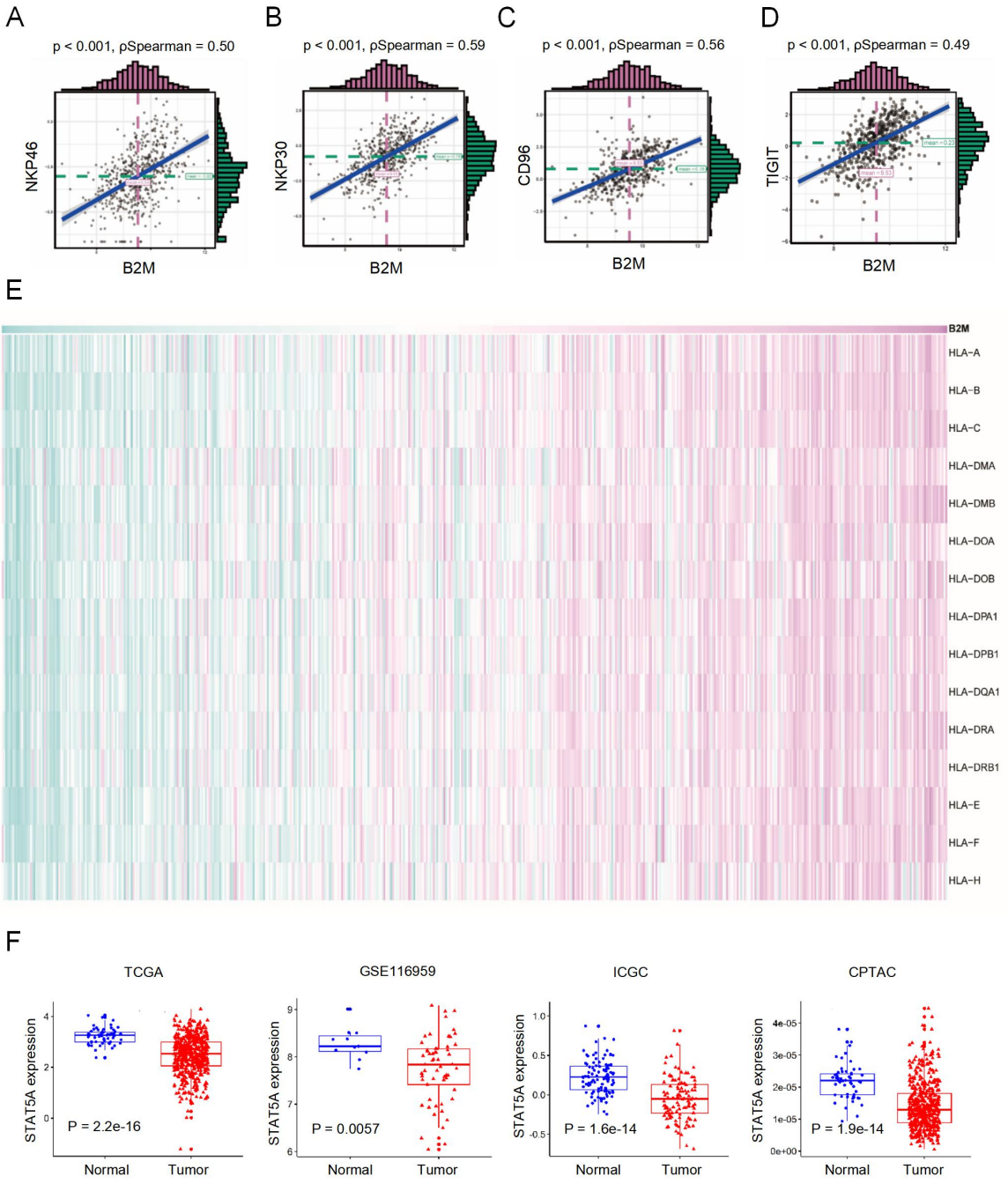

Figure S5. The relationship between B2M levels and NK cell recruitment and activation. (A-D) Positive correlations between B2M and the NK cell markers NKP46 and NKP30 and the NK cell-associated checkpoint molecules CD96 and TIGIT. (E) The correlation between the levels of B2M and HLA-I molecules. (F) STAT5 levels in LUAD tumor tissues compared with normal tissues in the LUAD, GSE116959, ICGC, and CPTAC datasets.

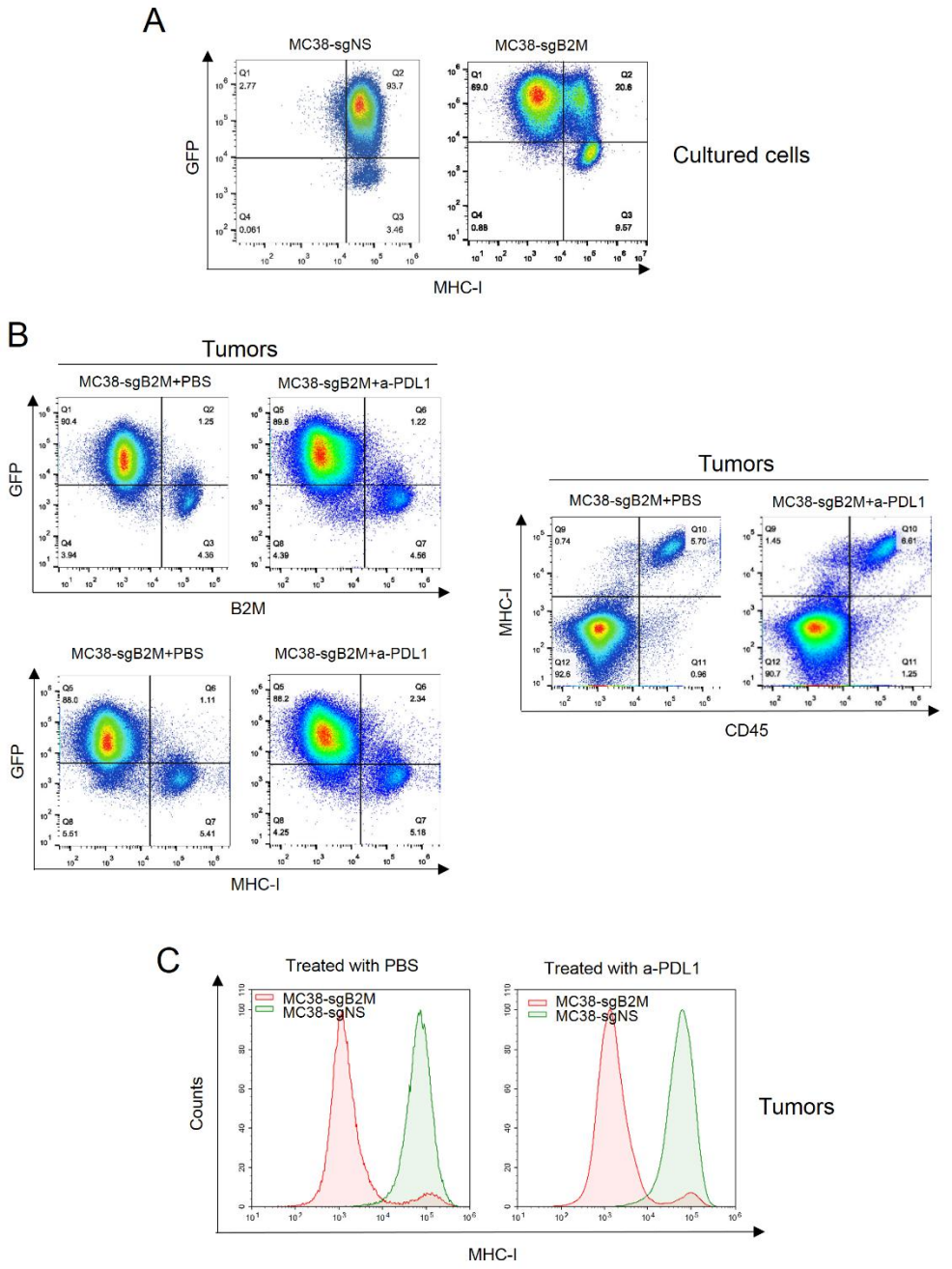

Figure S6. The expression of B2M and MHC class I on MC38 cells in vitro and in vivo. (A) FACS analysis of MHC class I on cultured MC38-sgNS and MC38-sgB2M cells in vitro. (B) FACS analysis of single-cell suspensions from MC38-sgB2M tumors treated with PBS or anti-PD-L1 for the expression of B2M, MHC class I, and CD45. (C) FACS analysis of single-cell suspensions from MC38-sgNS and MC38-sgB2M tumors treated with PBS or anti-PD-L1 for the expression of MHC class I.

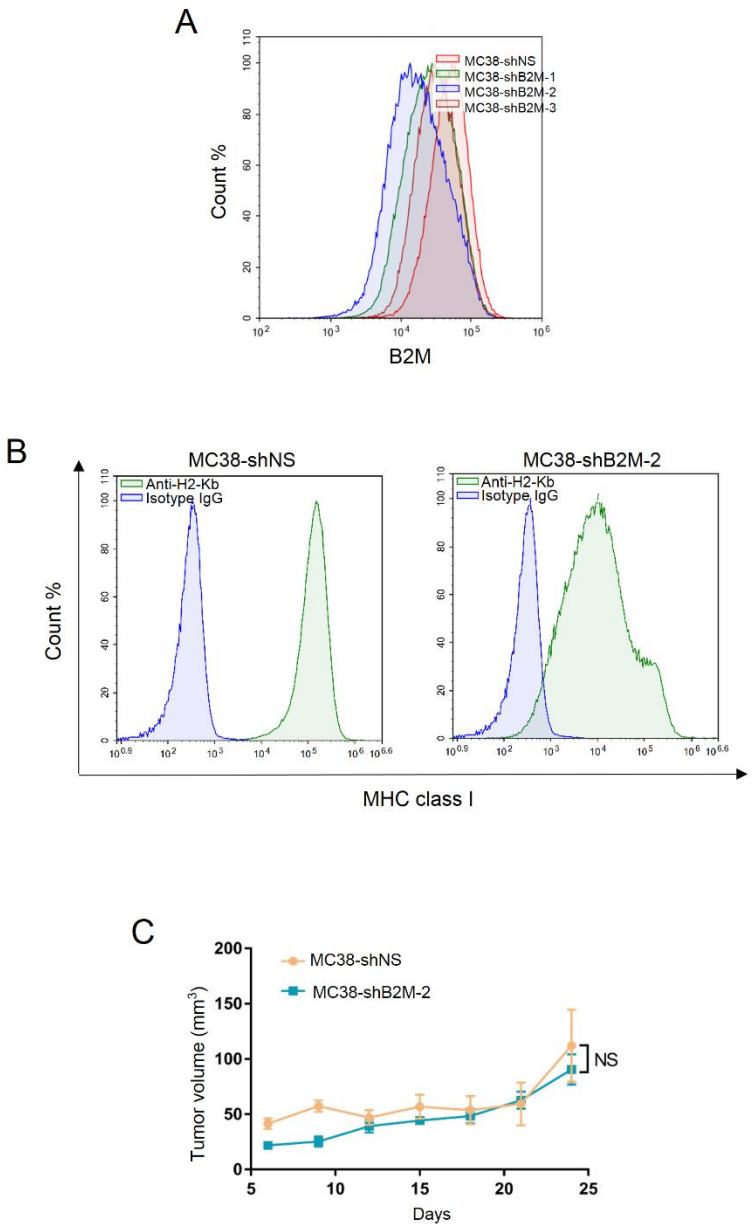

Figure S7. Inhibition of B2M expression in MC38 models. (A) FACS analysis of B2M on cells infected with lentivirus carrying nonspecific shRNA or shRNAs targeting B2M; the maximal inhibition of B2M cell surface expression was seen in MC38-shB2M-2 cells. (B) FACS analysis of MHC class I on MC38-shNS and MC38-shB2M-2 cells. (C) Subcutaneous tumors derived from MC38-shB2M-2 and MC38-shNS cells grew at a similar rate in vivo.

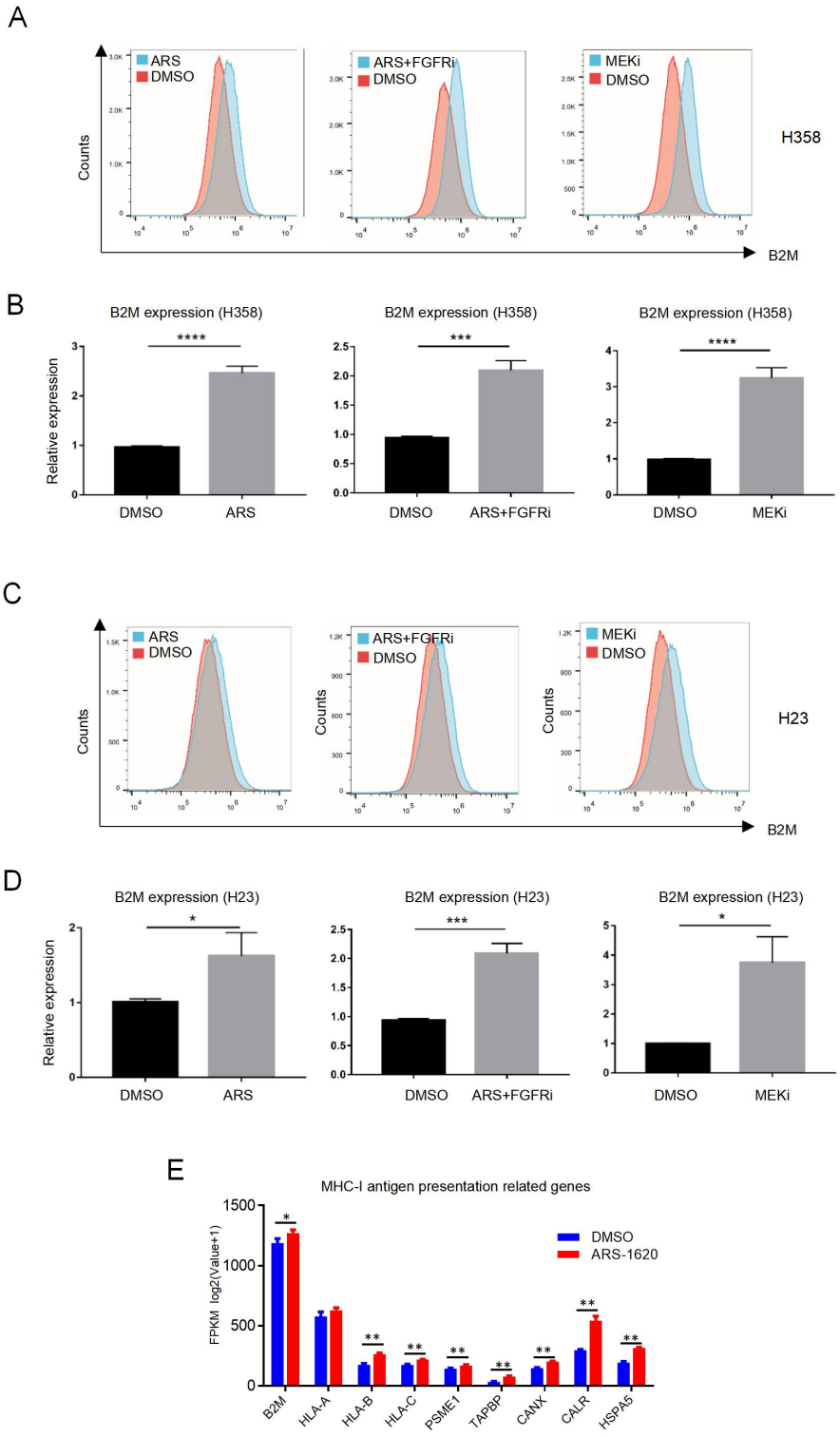

Figure S8. Mutant KRAS inhibition upregulated B2M expression in lung cancer cells. (A) FACS analysis of B2M on H358 cells treated with ARS-1620, ARS-1620+FGFR inhibitor

(FGFRi), or ERK inhibitor (ERKi) for 24 h compared with cells treated with DMSO. (B) Real-time PCR was used to determine the transcript levels of B2M in H358 cells treated with the indicated drugs for 24 h. (C-D) Similar experiments were conducted with H23 cells, as shown in Figure S7A and S7B. (E) RNA-seq data demonstrating the levels of the genes involved in antigen processing and presentation in H358 cells treated with ARS-1620 or DMSO for 24 h.